17 Interface Circuitry and Microsystems

Piero Malcovati
Department of Electrical Engineering, University of Pavia, Pavia, Italy

Franco Maloberti
Department of Electronics, University of Pavia, Italy

17.1 INTRODUCTION

Sensing physical or chemical quantities is a fundamental task in information processing and control systems. A sensing element or transducer converts the quantity to be measured into an electrical signal, such as a voltage, a current, or a resistive or capacitive variation. The data obtained from the transducers then have to be translated into a form understandable by humans, computers, or measurement systems. An electronic circuit called a sensor interface usually performs this task. The functions implemented by a sensor interface can range from simple amplification or filtering to A/D conversion, calibration, digital signal processing, interfacing with other electronic devices or displays, and data transmission (through a bus or, recently, through a wireless connection, such as Bluetooth).

Very-large-scale integration (VLSI) technologies have been extensively used to make sensor interface circuits since the appearance of the first integrated circuit (IC) in the early 1960s. Most of the sensor systems realized so far consist of discrete sensors combined with one or more application-specific integrated circuits (ASICs) or commercial components on a printed circuit board (PCB) or hybrid board. Over the past few years, however, progress in silicon planar technologies has allowed miniaturized sensors (microsensors) to be realized by exploiting the sensing properties of IC materials (silicon, polysilicon, aluminum, silicon oxide, and nitride) or additional deposited materials (such as piezoelectric zinc oxide, sensitive polymers, or additional metallization layers).

When microsensors are realized using IC technologies and materials, it is possible to integrate the interface circuit and several sensors on the same chip or in the same package, leading to microsystems or micromodules.[1-6] The potential advantages of this approach are numerous: The cost of the measurement system is greatly reduced due to batch fabrication of both the sensors and the interface circuits; its size and interconnections are minimized; and its reliability is improved.

However, the choice of materials compatible with silicon IC technologies is limited and their properties are process-dependent. Therefore, integrated sensors often show worse performance than their discrete counterparts due to weak signals and to offset and nonlinear transfer characteristics; they increase demands on interface circuits.

Moreover, in several sensor applications (such as automotive, biomedical, environment monitoring, and industrial process control), the chip or the chips (in the same package) containing microsensors and interface circuits can be exposed to harsh environmental conditions, causing aging and degradation of on-chip electronic devices. This makes most circuit techniques, which rely on accurate component matching and complex analog functions, inconvenient for sensor applications.

Given these considerations, it is evident that microsensor interface features can be very diverse. They depend heavily on the quantity to be measured, the physical effect used, the system architecture, and the application. In any case, it is very important that the microsensor, the interface circuit, and often the package are designed together. Indeed, the optimum microsystem or micromodule is not necessarily obtained by interconnecting separately optimized sensors and interface circuits. Microsensor interface circuit design, therefore, requires specific and interdisciplinary knowledge as well as special techniques to achieve the reliability and performance demanded by the user.

Finally, profitable use of smart sensors in real products not only depends on good design; it is also related to a number of additional issues such as cost-effective production, packaging, and post-production testing. All these issues are considered in this chapter.

17.2 MICROSENSOR SYSTEMS

There are two possible approaches for implementing microsensor systems: the microsystem approach and the micromodule approach. In the microsystem approach, the sensor and the interface circuitry are integrated on the same chip, as shown in Fig. 17.1. In this case, the whole system is realized using a fabrication process optimized for integrated circuits with a few compatible post-processing steps when necessary (typically, etching or deposition of materials). Therefore, the microsensor must be designed by taking into account the material characteristics (layer thickness, doping concentrations, and design rules) given by the standard IC process used (bipolar CMOS, BiCMOS) and any specific processing step has to be performed after the completion of the standard IC fabrication flow. Obviously, this situation reduces the degrees of freedom available for optimizing sensor performance, thus making the design more challenging. This approach also can raise cost and yield issues, especially when using modern technologies with small

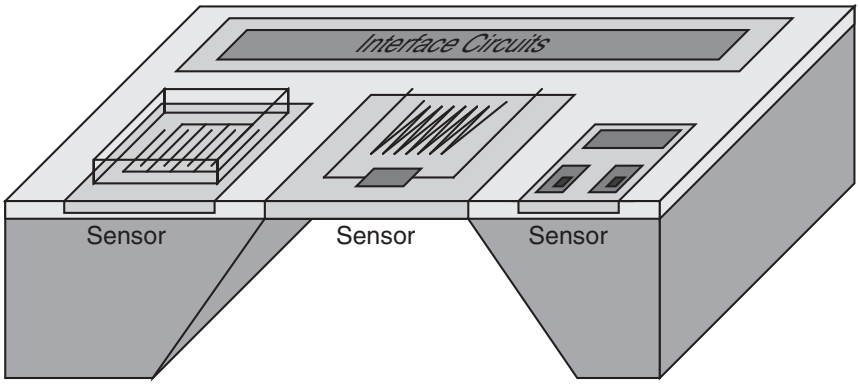

Figure 17.1 Microsensor system realized using the microsystem approach.

feature size (submicron technologies). In fact, while the silicon area occupied by the interface circuit is typically shrinking, together with the feature size of the technology, the sensor area in most cases remains constant. This is because it is determined by physical considerations, such as the mass of the structures or the angle of etched cavities, which are not changed by improvements in the technology. Therefore, while for integrated circuits the increasing cost per unit area is abundantly compensated by the reduction in the area, leading to an overall reduction of chip cost with the technology feature size, this might not be true for integrated microsystems. Moreover, a defect in the sensors may force us to discard the complete microsystem, even if the circuitry is working, thereby lowering the yield and again increasing the cost. (The yield for sensors is typically lower than for circuits.)

The microsystem approach also has considerable advantages. First, the parasitics due to the interconnections between the sensors and the interface circuitry are minimized and, more important, are well-defined and reproducible; this is very beneficial for system performance. In addition, the system assembly is simple, inexpensive, and independent of the number of connections needed, since all the interconnections are implemented during the IC fabrication process. Finally, when required, the use of the same technology allows us to achieve good matching between elements of the sensor and those of the interface circuitry, allowing accurate compensation of many parasitic effects.

In the micromodule approach, the sensors and the interface circuitry are integrated on different chips. They are included in the same package or mounted on the same substrate, as shown in Fig. 17.2. The interconnections between the sensor chip and the interface circuit chip can be realized with bonding wires or other techniques, such as flip-chip or wafer

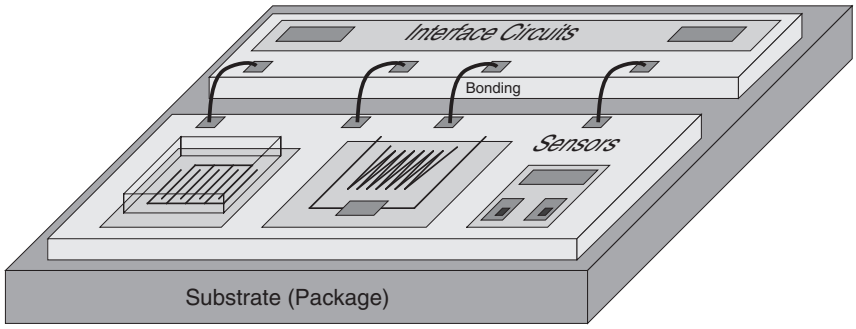

Figure 17.2 Microsensor system realized with the micromodule approach.

bonding. With this approach, the two chips can be fabricated with two different technologies, which are optimized for the sensors and the circuitry, respectively. Typically, expensive submicron technologies are adopted to realize interface circuitry, while low-cost technologies with large feature size and few masks are used for implementing sensors. Therefore, the sensor designer can adjust the material properties of the technology to optimize the performance of the devices, and the cost and yield issues mentioned for the microsystem approach are no longer a concern.

However, the micromodule approach also has a number of drawbacks. First, the assembling of the system can be quite expensive and a source of possible failures, and the number of interconnections allowed between the sensor and the circuitry is limited. Moreover, the parasitics due to the interconnections are some orders of magnitude larger, more unpredictable, and less repeatable than in the microsystem approach, thus destroying in many cases any improvements obtained in sensor performance by technology optimization. Finally, matching between elements of the sensor and elements of the interface circuitry cannot be guaranteed.

The advantages and disadvantages of both approaches are summarized in Table 17.1. From the considerations just discussed, it is evident that both approaches have merits. The choice of the approach to follow depends substantially on the application, the quantity to be measured, the kinds of sensors, the specifications of the interface circuits, and the available fabrication technologies, thus producing a number of tradeoffs that must be analyzed before a decision is made. For example, Fig. 17.3 illustrates the tradeoff between IC technology feature size and microsensor system cost. It can be clearly deduced from the indicative figures shown that if the sensor cost is constant, the microsystem approach is more convenient for technologies with large feature size, while the micromodule approach is more suitable for technologies with small feature size.

Table 17.1 Comparison Between the Microsystem and Micromodule Approaches

Microsystem Approach	Micromodule Approach
+ Reliability	+ Optimal yield
+ Minimal interconnection parasitics	+ Optimal processes for both sensors and circuitry
+ Simple and inexpensive assembling	+ Cost that scales with feature size
– Reduced yield	– Reliability
– Cost that does not scale with feature size	– Large interconnection parasitics
– Optimal process only for sensors	– Complex and expensive assembly

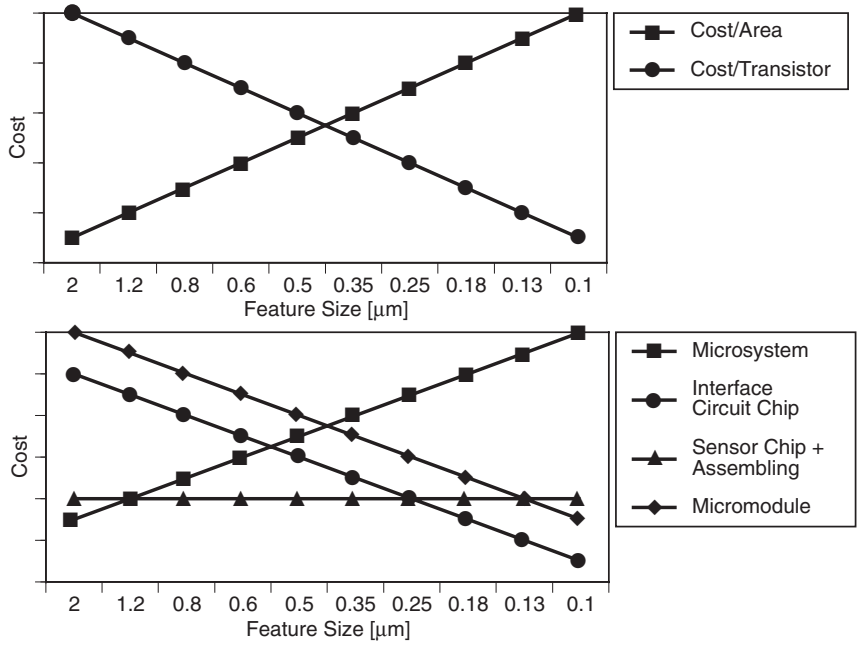

Figure 17.3 Tradeoff between IC technology feature size and integrated microsensor system cost.

17.3 MICROSENSOR SYSTEM APPLICATIONS

As mentioned earlier, microsensor systems are currently replacing discrete sensors in a number of areas because of their inherent advantages; namely, batch fabrication, low cost, high reliability, and on-chip signal processing. In sensing applications, however, the environments where systems

have to operate may be substantially different from the controlled and "mild" settings enjoyed by conventional integrated circuits. Sensors must be placed close to the quantity to be monitored; for example, in the human body, in an engine, or in an aggressive atmosphere. The operating environment of microsensor systems can consequently be both harsh and hostile. This introduces additional demands on the performance of integrated circuits, especially robustness. It is therefore useful to systematically consider the specific environmental conditions and requirements associated with the application areas where microsensors may be used (Table 17.2).

Table 17.2 Microsensors by Application Environment

	Quantity to Measure	
Application	**Physical**	**Chemical**
Automotive	• Acceleration • Flow • Magnetic field • Temperature • Pressure • Radiation • Images	• Exhaust gas composition • Combustion control • Air quality
Biomedical	• Pressure • Flow • Temperature • Acceleration • Magnetic field • Viscosity	• Biochemical species • Ionicity • Composition of body liquids
Household Appliances, Building Control, and Industrial Control	• Flow • Pressure • Acceleration • Magnetic field • Temperature • Radiation • Images • Viscosity	• Humidity • Gas composition • Liquid composition
Environmental	• Flow • Pressure • Temperature • Radiation • Images • Viscosity	• Gas composition • Liquid composition • Humidity • Biochemical compounds • Ionicity

17.3.1 Automotive Sensors

The number of sensors used in modern cars is growing because of government regulations and market expectations.[7-9] High fuel efficiency, clean emissions, improved safety, and comfort are the most important functions requiring on-board sensors. Moreover, because of the increasingly large number of parts per year involved, sensors for the automotive market must be extremely low priced. Automotive environmental conditions, summarized in Table 17.3, are especially difficult to address. Sensors can be placed inside the engine or outside the car, where they are subject to extreme temperature cycles, mechanical shocks, electromagnetic interference, and aggressive chemicals. Nevertheless, automotive sensors, like other car components, are required to be reliable and maintain their accuracy for 5 to 10 years.

It is evident from these considerations that automotive microsensor interface specifications are quite severe, making circuit design very challenging. An example of a microsensor system already introduced in the automotive market is the air-bag accelerometer.[10,11] In this case, special functions such as self-test, calibration, and bus interface have been included in the system.

Systems for engine emission and combustion control, based on microsensors, are also being developed.[12-17] They combine physical and chemical sensors that measure the state of the engine; for example, pressure in the cylinder, oxygen content in the exhaust gases, and engine rotation speed. These data are processed and used to regulate spark ignition and fuel injection, to optimize the performance of the engine in terms of fuel consumption and pollution.

Table 17.3 Microsensor Environment in Automotive Applications

Environmental Condition	Value
Temperature	• –40 to 150° C
Acceleration	• > 50 g
Vibrations	• > 15 g
Exposure to:	• Fuel
	• Brake fluid
	• Oil
	• Transmission fluid
	• Salt
	• Water
Electromagnetic Interference	• 200 V/m

17.3.2 Biomedical Sensors

Miniaturization and low power consumption are very important for biomedical and, in particular, implantable sensors. Microsensor technology is therefore very well suited for this type of application. Implantable microsystems or micromodules are indeed being developed for invasive monitoring of patients as well as for delivering electrical and chemical stimuli to the body.[18-23]

The specifications for implantable systems are very stringent. Low-voltage and low-power operation is imperative to ensure sufficiently long battery duration. The highest degrees of reliability and stability are required since substitution of a failed device requires surgical intervention and, in the worst case, a failure could be fatal. Packaging is crucial to protect the system from aggressive body fluids (such as blood) and vice versa. Finally, communication between the implanted system and the external world is limited, since only very few direct contacts are allowed.

Pacemakers are an important application of implantable microsensor systems. These devices are used to treat cardiac arrythmias such as bradycardia (slow heart rate) and tachycardia (rapid heart rate) by assisting the heart's natural pacemaking function with voltage pulses (5 to 10 V). Communication with the external world is provided by an inductive telemetry system operated at low frequencies or a transceiver, including an antenna, operated at radio frequencies. In some cases, the telemetry system also provides the power supply.[21,22]

17.3.3 Sensors for Household Appliances, Building Control, and Industrial Control

Electronic components, including sensors, are becoming more numerous and complex in modern white goods. Control systems for washing machines, ovens, air conditioning systems, alarm systems, vacuum cleaners, industrial process control, and so forth all require sensing elements. Sensor specifications in the industrial, household, and automotive markets are somewhat similar because of the large number of parts per year involved and the comparable environmental conditions (Table 17.3). In many cases, however, sensors for the household market must be particularly cheap, because the added value of the whole set of equipment is relatively low.

Recently, a number of microsensor systems for white goods have been proposed,[24-26] including flow sensors (for vacuum cleaners and air conditioning systems), temperature sensors (for ovens, washing machines, and air conditioning systems), magnetic sensors (for contactless switches), chemical sensors, and infrared sensors (for alarm systems).

17.3.4 Environmental Sensors

The release of various chemical pollutants into the atmosphere from industries, automobiles, and buildings, and into the hydrosphere causes environmental problems such as acid rain, greenhouse effect, ozone depletion, and polluted water. Microsensor systems for environmental monitoring are therefore being investigated.[27-29] The concentration of pollutants to be detected is usually quite small (in the parts-per-million range), and the selectivity of chemical microsensors is usually limited. This leads to tough specifications for on-chip interface circuits. Special nonlinear signal processing algorithms such as fuzzy logic and neural networks are widely used because by combining signals from several sensors, they allow significant information to be extracted, even in the presence of crosstalk and noise.

17.4 INTERFACE CIRCUIT ARCHITECTURE

Figure 17.4 shows the block diagram of a generic microsensor interface circuit. This kind of architecture is valid for microsensor systems implemented with either the microsystem or the micromodule approach. In addition to the sensors, the system includes some analog front-end circuits (amplification and low-level processing), one or more analog-to-digital (A/D) converters, a digital signal processor, and an output interface.

It is well known that signal processing in the digital domain is more robust than in the analog domain thanks to the larger noise margin. Therefore, although processing is performed more efficiently with analog tech-

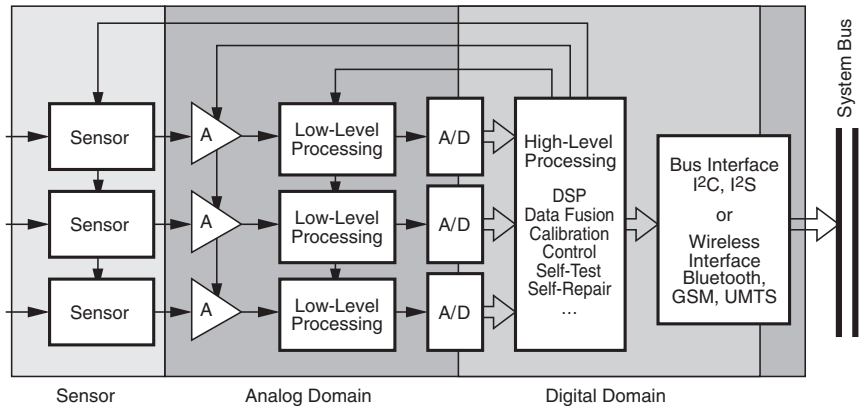

Figure 17.4 Block diagram of a generic microsensor interface circuit.

niques, in the presence of harsh environmental conditions, the trend is to minimize the analog section, moving the A/D converter toward the input and leaving complex processing to the digital section. This means that the overall performance of the system becomes strongly dependent on the quality of the A/D converter. Moreover, since less analog signal processing is performed, the bandwidth and dynamic range specifications for the A/D converter itself become more severe.

In the block diagram of Fig. 17.4, it is interesting to note the presence of feedback signals from the digital processor to the sensors and analog front-end, which allow the performance to be optimized by adjusting system parameters, depending on the output signal. For example, it is possible to correct the offset of the system by adjusting the reference voltages or to optimize the dynamic range by changing the gain of the analog front-end.

17.4.1 Requirements and Specifications

Sensor systems often emulate some kind of human sensing. Therefore, the properties of the electrical signals generated are related to the characteristics shown by natural perception: a relatively small bandwidth and quite a large dynamic range (often over a logarithmic span). Processing this kind of signal is usually not particularly difficult. However, when the dynamic range is large, noise contamination may become a problem. In this case, low-noise amplification and filtering, strictly limited to the band of interest, are necessary.

System specifications depend on both the function to be implemented and the application itself. Very often, however, a real-time response is required. In the case of human-like sensing, real-time means that a few milliseconds will always be available to process the signals; therefore, this is not a problem. By contrast, for control or recognition of fast-moving objects such as cars or planes, real-time can imply several megahertz of bandwidth.

Electronic equipment is becoming more and more portable, leading to battery-operated sensor systems with a small volume and weight. These features imply microsensor technologies, special packaging and assembling, low-voltage and low-power design methodologies, robustness, and shock resistance. For special cases (for example, in implanted devices, hearing-aids, or smart cards), it is also necessary to extract the power required for system operation from an electromagnetic flux irradiating the system itself. In this case, microactuators must be included in the system.

Before discussing the different sensor interface blocks in detail, it is useful to provide a sensor classification from the interface circuit point of view. The first parameter is the kind of output signal: current, voltage, or variation of resistance, capacitance, or inductance, as summarized in

Table 17.4. We can also consider different subclasses of sensors on the basis of signal level, bandwidth, and biasing requirements.

Table 17.5 provides critical parameters and tasks resulting from typical microsensor system specifications. It highlights challenging figures for signal level and bandwidth, and confers an immediate awareness of the difficulties to be faced in interface circuit design.

Table 17.4 Microsensors by Electrical Output Signal

Output Signal	Physical or Chemical Effect	Quantity to Measure	
		Physical	**Chemical**
Voltage	Pyroelectric	• Infrared radiation	• Reaction enthalpy
	Piezoelectric	• Strain • Acceleration • Pressure • Viscosity	• Gas composition • Liquid composition
	Thermoelectric	• Temperature • Infrared radiation • Flow • AC power	• Reaction enthalpy
	Hall	• Magnetic field	
Current	Lorentz	• Magnetic field	
	Photoelectric	• Radiation • Particles	• Gas composition • Liquid composition
	ISFET		• Ionicity • Liquid composition • Biochemical species
Capacitance	Dielectric permittivity variation		• Gas composition • Humidity • Biochemical species
	Dielectric thickness variation	• Strain • Acceleration • Pressure	• Humidity
Resistance	Piezoresistive	• Strain • Acceleration • Pressure	
	Magnetoresistive	• Magnetic field	
	Resistivity variation	• Temperature • Pressure • Flow • AC power	• Reaction enthalpy • Gas composition • Liquid composition

Table 17.5 Microsensor Interface Challenges

Classification	Parameter/Task	Challenges
Output Signal	• Analog voltage • Analog current • Change of resistance • Change of capacitance	• 10 μV • 10 nA • 1 mΩ • 10 aF
Operation	• Buffer • Amplification • Biasing • Filtering	• Low offset (100 μV) • Low noise (nV) • Low drift over time • 0.1% accuracy over temperature • Low cutoff frequency
Additional Functions	• Linearization • Self-test • Digital correction • Low power • Digital programming • Bus interface • Wireless interface	

17.5 ANALOG FRONT-END

The analog-front end of a microsensor interface circuit, directly connected to the sensing element, has to transform the raw sensor signal into something suitable for the subsequent A/D converter. The functions implemented in the analog front-end are typically limited to amplification and filtering, leaving more complex signal processing tasks to the digital section. Since the analog-front end is directly connected to the sensor, its features depend strongly on the kind of sensor considered. In this section, we consider in detail the characteristics of the analog front-end for sensors that provide voltage output, current output, or impedance variation.

17.5.1Voltage Output

A wide variety of possible microsensors provide voltage output, typically including pyroelectric, thermoelectric, and piezoelectric devices; transistor-based temperature sensors; and magnetic sensors based on the Hall effect. Depending on specifications and applications, one of a variety of analog front-end circuits should be adopted. When the output signal of

the sensor is sufficiently large (in the millivolt range) and noise is not a main concern, standard operational or instrumentation amplifiers, together with continuous-time or switched-capacitor filters, are sufficient. These solutions are quite conventional and require only customary design know-how. This task is made easier by libraries of standard analog cells, which are often provided by silicon foundries.

Situations in which the signal level approaches the limit given in Table 17.5 are much more challenging. Custom interface circuits must be designed, and special care must be taken to address noise and offset rejection. Bipolar transistors and high power supply voltages help to solve noise problems. Low-voltage supplies of 5 or 3.3 V (or even lower for portable equipment) in CMOS technology are an even more critical constraint.

Before discussing a specific interface implementation, we will recall the noise power spectral density of a simple MOS transistor. This is given by

$$S_{V_n} = \underbrace{\frac{8kT}{3g_m}}_{\text{Thermal}} + \underbrace{\frac{k_F}{2\mu f^{\alpha} C_{ox}^{k+1} WL}}_{\text{Flicker}}, \tag{1}$$

where g_m is the transconductance of the device, W and L are the gate dimensions, C_{ox} is the specific capacitance of the gate, k is the Boltzman constant, T is the absolute temperature, μ is the mobility of the channel, f is the frequency, and k_F is the flicker noise coefficient.

Equation (1) shows how to minimize noise contributions. The white thermal part is reduced by increasing the transconductance (at the expense of power consumption and DC gain, while improving speed), whereas flicker noise, which is higher than in bipolar devices because conduction takes place near the Si/SiO_2 interface, can be curtailed by increasing the gate area. When power and area consumption are critical parameters, however, noise should be reduced at the system level. When low-frequency noise (1/*f*) is the main concern, one of the following techniques is normally used:

- Auto-zero or correlated double sampling[30,31]
- Chopper stabilization[32, 33]

The auto-zero or correlated double sampling technique reduces the offset and low-frequency noise at the system level.[34,35] This technique requires sampled data operation. The low-frequency noise and the offset are, in fact, canceled in two steps, during two nonoverlapping clock phases. In

the first step, the input signal (V_S) is disconnected from the circuit, and the spur signal (V_N) is sampled and stored. In the second step, V_S is connected to the circuit, and the previously stored spur component ($V_N\ z^{-1}$) is subtracted from the corrupted signal ($V_S + V_N$). If A is the gain of the circuit, the resulting transfer functions are ideally $H_S = A$ for the input signal, and

$$H_N = A\left(1 - z^{-1}\right) = 2A\sin\left(\frac{\pi f}{f_S}\right), \tag{2}$$

where f_S denotes the sampling frequency for the offset and the noise. Therefore, if $f_S \gg B$, and B denotes the bandwidth of the input signal, the in-band noise component is strongly attenuated. A practical implementation of this technique is reported by Malcovati *et al.*[36] The most important features of this circuit are summarized in Table 17.6.

The operating principle of the chopper stabilization technique is illustrated in Fig. 17.5.[37,38] A noisy operational amplifier with noise corner frequency f_{Corner} is preceded and followed by two identical modulators. The input signal, modulated with a square wave (Ck) having a frequency larger than f_{Corner}, is shifted into a region of the spectrum where the noise of the amplifier is dominated by the thermal component. After amplification, the signal is then modulated again and shifted back into the original band. The offset and the large low-frequency noise of the amplifier, superimposed on the signal by the amplification process, are also modulated and, therefore, pushed to a high frequency, where they can be removed by a subsequent low-pass filter.

This technique is often used in continuous-time systems, since it does not require sampled signals and allows quite good noise figures to be obtained. However, because of operational amplifier nonlinearities, the harmonics of the square wave may give rise to intermodulation products in the

Table 17.6 Features of the Low-Noise Operational Amplifier Based on the Auto-Zero Technique Reported by Malcovati *et al.*[38]

Parameter	Value
Application	Infrared thermoelectric sensor
Input referred noise	5 μV_{RMS}
Input referred offset voltage	1 μV
Bandwidth	10 Hz
Gain	Programmable

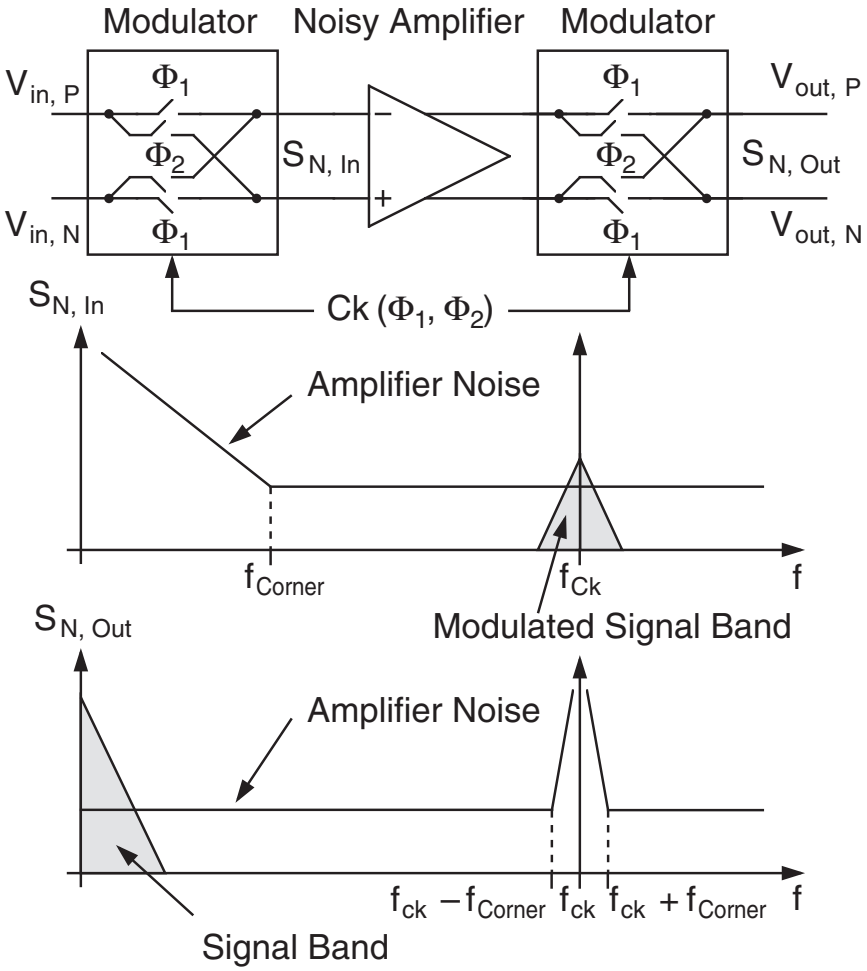

Figure 17.5 Operating principle of a low-noise operational amplifier based on the chopper stabilization technique.

signal band and degrade the noise performance of the circuit. Therefore, the operational amplifier has to be designed very carefully, possibly with a bandpass transfer function, to filter the offset and the high-order harmonics.

One of the best implementations of the chopper stabilization technique for microsensor applications is reported by Schaufelbühl *et al.*[39] and Menolfi and Huang.[40] The most important features of this circuit are summarized in Table 17.7.

Table 17.7 Features of the Low-Noise Operational Amplifier Based on the Chopper Stabilization Technique Reported by Schaufelbühl *et al.*[39] and by Menolfi and Huang[40]

Parameter	Value
Application	Infrared thermoelectric sensor array
Input referred noise	260 nV_{RMS}
Input referred offset voltage	600 nV
DC gain	77 dB
Bandwidth	600 Hz
Chopper frequency	11 kHz

17.5.2 Current or Charge Output

Sensors that provide a current output include particle detectors, optical sensors, ion-sensitive field effect transistors (ISFET), and magnetic sensors operated in the current (Lorentz) mode. The sensor currents can range from a few picoamperes to several microamperes. Charge preamplifiers are commonly used for very low currents (for example, in particle detectors).[41-48] Since a long integration time is required, the bandwidth of these circuits is quite small.

A typical structure of a charge preamplifier is shown in Fig. 17.6. Circuit operation is divided into two phases. First, the charge on the photodiode is integrated on capacitor C_F while the voltage across the

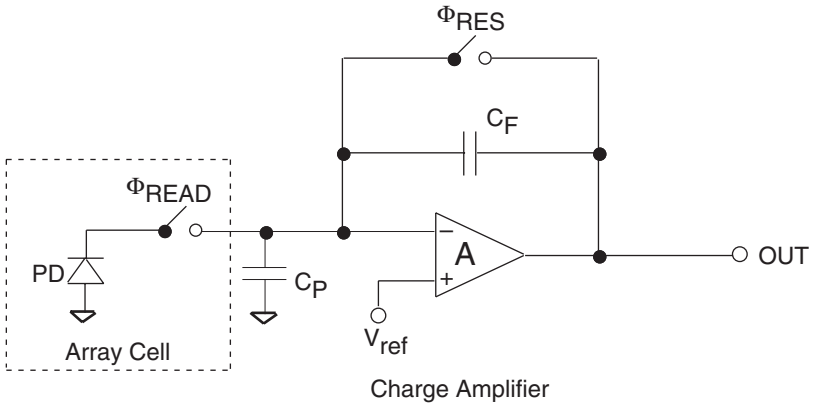

Figure 17.6 Schematic of a typical charge amplifier.

photo-diode approaches V_{ref} (Φ_{READ} closed and Φ_{RES} open). Then, capacitor C_F is discharged (to be ready for a new sample), setting the photodiode voltage at V_{ref}(Φ_{READ} closed and Φ_{RES} closed). The error caused by the offset of the gain stage A is canceled because it is stored on C_P during Φ_{RES}.

In relatively wideband applications, nonintegrating transimpedance or current amplifiers should be used.[48-56] These circuits can achieve large amplification, but noise is a critical issue, especially when bipolar transistors are not available.

When the output current is sufficiently large, we can exploit the sensor to replace an active component (such as a current source) in an A/D converter or in a filter, thus minimizing the complexity of the system. In sampled data systems, the switched-current technique[57] can be used to implement auto-zeroed low-noise current amplifiers. In spite of some drawbacks that have not yet been fully solved (namely, charge injection and nonlinearity), this approach deserves further investigation, especially for low-voltage (battery-operated) applications.

As examples, we can consider the charge amplifier reported by Simoni *et al.*[58] and the current amplifier implemented in bipolar technology discussed by Bolliger *et al.*[59] The most important features of these two circuits are reported in Tables 17.8 and 17.9, respectively.

The schematic current amplifier designed for UV sensing applications[59] is shown in Fig. 17.7. The UV photodiode current and the DC bias

Table 17.8 Features of the Charge Amplifier Reported by Simoni *et al.*[58]

Parameter	Value
Application	CMOS digital camera
Dynamic range	82 dB
Input referred noise	780 electrons
Sensitivity (including photodiode)	4 lux

Table 17.9 Features of the Current Amplifier Reported by Bolliger *et al.*[59]

Parameter	Value
Application	Bipolar UV sensor
Input range	20 pA to 1 nA
Transresistance gain	0.95 GΩ
Bandwidth	20 Hz
Input referred noise	16.5 pA_{RMS}

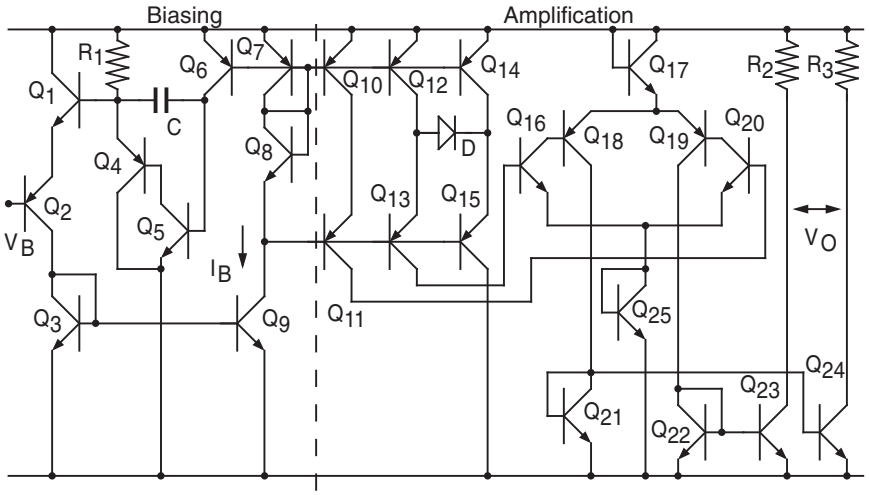

Figure 17.7 Schematic of the current amplifier reported by Bolliger *et al.*[59]

current (I_B) are amplified by the current gain (β) of transistors Q_{16} and Q_{18}. Moreover, a replica of I_B is also amplified by transistors Q_{19} and Q_{20}. The resulting currents, properly mirrored (Q_{21}, Q_{22}, Q_{23}, and Q_{24}), are transformed into voltage by R_3 and R_2. The left part of the circuit generates a suitable DC bias current by means of a feedback loop. Voltage V_B allows I_B to be controlled in the range of 5 to 15 nA. Assuming perfect element matching, the output voltage of the circuit can be expressed as

$$V_O = \beta_{16}\beta_{18}KR_3I_D. \tag{3}$$

With β around 200, R_3 = 20 kΩ, and a mirror factor K equal to 2, a transresistance gain of about 10^9 Ω can be achieved.

17.5.3 Impedance Variation

Silicon technologies allow a variety of resistive or capacitive structures whose value is controlled by a physical or a chemical quantity to be fabricated. Resistive sensors are usually based on piezoresistive effects (resistance variations due to stress in the material) or thermal effects (resistivity of conductors changes with temperature). Examples are strain gauges, piezoresistive pressure sensors, resistive Pirani gauges, and temperature sensors. Moreover, chemical sensors can be realized from mate-

rials whose conductivity changes according to the absorption of ambient gases. In contrast, capacitive microsensors are based on the variation in the permittivity or in the thickness of the dielectric layer of a capacitor induced by a physical or chemical quantity. Humidity, chemical compounds, pressure, and acceleration sensors can all be realized with this approach. The magnitude of the capacitive variation can range from hundreds of attofarads to a few picofarads.

DC Wheatstone bridges are frequently used to transform resistance variations into voltages and compensate for parasitic effects. Referring to Fig. 17.8, the output voltage of the bridge is given by

$$V_{out} = \left(\frac{Z_1}{Z_1 + Z_2} - \frac{Z_3}{Z_3 + Z_4} \right) V_{ref} . \tag{4}$$

The amplitude of the bridge output signal depends on the magnitude of the resistive variation, which can range from a few milliohms to several hundreds of ohms. The whole bridge network, therefore, can be considered as a sensor providing voltage output.[60-62] When it is not possible or convenient to realize a bridge structure, a resistive sensor may replace any resistor in a circuit, which can therefore deliver an output signal sensitive to the quantity to be measured. For example, it is possible to design an RC oscillator whose output frequency is tuned by the resistive sensor.[63-65]

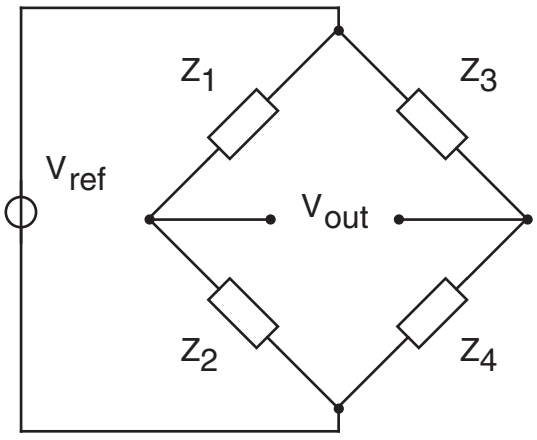

Figure 17.8 Schematic of the Wheatstone bridge.

Capacitive sensors can be read out with an AC bridge or used to build an oscillator. In CMOS technology, it is possible to place the sensor directly in a switched-capacitor circuit, as shown in Fig. 17.9.[66-70] In this circuit, the output voltage at the end of clock phase Φ_2 is given by

$$V_{out} = \frac{1}{C_2}\left(C_{1s}V_{sen} - C_{1r}V_{ref}\right), \tag{5}$$

where C_{1s} is the sensor and C_{1r} is a reference capacitor equal to the sensor but not sensitive to the quantity to be measured. By choosing suitable values for C_2, V_{sen}, and V_{ref}, it is possible to detect capacitance variations on the order of tens of attofarads (1 aF = 10^{-18} F).[71]

A practical implementation of this technique is reported by Gola *et al.*[72] The most important features of this circuit are summarized in Table 17.10.

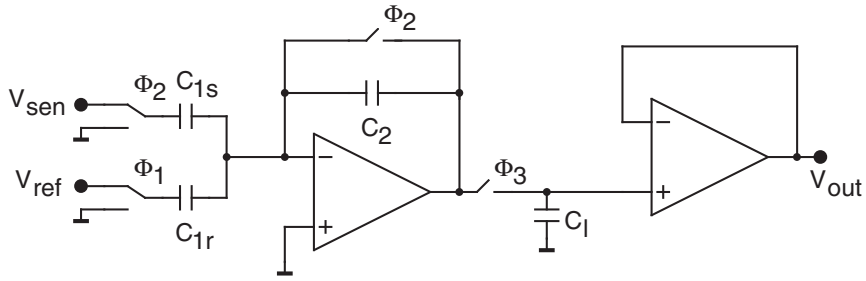

Figure 17.9 Switched-capacitor amplifier for capacitive sensors.

Table 17.10 Features of the Switched-Capacitor Interface for an Angular Accelerometer Reported by Gola *et al.*[72]

Parameter	Value
Application	Angular accelerometer
Resolution	2.5 rad/sec^2
Minimum capacitance variation	0.05 fF
Bandwidth	800 Hz

17.6 A/D CONVERTER

A/D converters are becoming the most critical components of microsensor systems because the signal processing is reduced in the analog domain. For example, consider a sensor providing a maximum output signal of 10 mV on top of an offset voltage of ±100 mV (which is the case for Hall devices, for example). If we want to resolve 0.1% step by connecting an A/D converter directly to the sensor and performing the offset cancellation in the digital domain, we need 14-bit resolution. But if we implement some sort of offset cancellation in the analog domain in front of the A/D converter, the required resolution drops to 10 bits.

Before considering the most popular A/D converter architectures in detail, from the microsensor interface circuit point of view, it is useful to recall briefly a few concepts and definitions. The digitalization of an analog signal, or A/D conversion, involves discretization in both time and amplitude. For band-limited signals, sampling at the Nyquist rate (twice the signal bandwidth, or baseband) allows the original signal to be represented fully without distortion. However, discretization in amplitude, or quantization, always introduces an error (quantization error). During the quantization process, in fact, the input signal x is approximated with the closest quantized value x_n, giving rise to the quantization error $Q = x - x_n$. By considering Q as a stochastic variable, we can analyze the quantization effect with statistical methods, exploiting the same mathematical tools commonly used to handle noise. The quantization error is, therefore, generally identified as quantization noise. The power of the stochastic variable $Q(P_Q)$ is given by its variance, according to

$$P_Q = \sigma_Q^2 = \int_{-\Delta/2}^{\Delta/2} Q^2 \psi(Q) dQ, \tag{6}$$

where Δ denotes the quantization step amplitude and $\psi(Q)$ is the probability density of Q ($-\Delta/2 < Q < \Delta/2$). Assuming $\psi(Q)$ to be uniform ($\psi = 1/\Delta$), P_Q is given by

$$P_Q = \frac{\Delta^2}{12}. \tag{7}$$

Moreover, the spectrum of the quantization noise is generally considered to be white in the frequency range between DC and the sampling frequency f_S.[73]

A straightforward way to reduce the quantization error is to increase the resolution of the quantizer, thus making the step size (Δ) smaller (Nyquist rate A/D converters). Another way is to reduce the fraction of the quantization noise in the signal band B by increasing f_S above the Nyquist rate (oversampling), as shown in Fig. 17.10 (oversampled A/D converters). In this case, the resulting in-band quantization noise power is given by

$$P_Q = \int_0^B \frac{\Delta^2}{6f_S} df = \frac{\Delta^2 M}{12}, \tag{8}$$

where $M = 2B/f_S$ is called the oversampling ratio. Naturally, a digital low-pass decimating filter must follow the oversampled A/D converter to eliminate the out-of-band quantization noise and resample the signal at the Nyquist rate.[74]

An overview of several different A/D converter architectures, both Nyquist rate and oversampled, with typical resolution and conversion time (expressed in number of clock cycles) is reported in Table 17.11.[75-115] The table also considers how well each architecture is suited to microsensor applications.

The use of Nyquist rate A/D converters is imperative in high-frequency applications, such as video processing or high-speed data transmission, because in these cases, oversampling would lead to an impractical speed of operation. Several architectures and algorithms are available to implement Nyquist rate A/D converters. The number of clock periods required to perform a complete conversion cycle and the corresponding hardware complexity are the most distinctive features of each architecture. For example, flash converters perform one conversion per clock period, but they require 2^N comparators and 2^N reference elements, N denoting the desired resolution. By contrast, successive approximation converters need N clock periods to complete one conversion, but they require only one comparator and N reference elements. Subranging, half-flash, and pipeline A/D converters need between two and N clock periods per conversion, with decreasing hardware complexity.

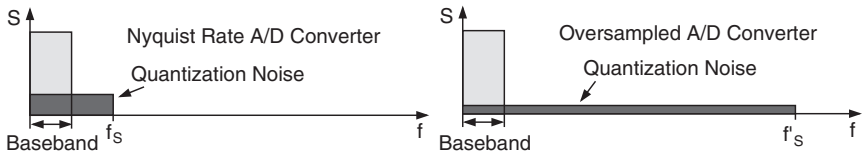

Figure 17.10 Signal and quantization noise spectra in Nyquist rate and oversampled A/D converters.

Table 17.11 Overview and Features of Different A/D Converter Architectures (N denotes the resolution, f_{ck} the clock frequency)

A/D Converter Architecture	Maximum Resolution	Conversion Time	Suitable for Microsensors
Nyquist Rate A/D Converters			
Flash A/D Converters[78-81]	6 bit	$1 / f_{ck}$	–
Subranging and Pipeline A/D Converters[82-86]	12 bit	$< N / f_{ck}$	=
Folding A/D Converters[87-88]	10 bit	$< N / f_{ck}$	–
Successive Approximation A/D Converters[89-92]	12 bit	N / f_{ck}	=
Algorithmic A/D Converters[93-95]	12 bit	N / f_{ck}	=
Oversampled A/D Converters			
Dual-Slope A/D Converters[96-97]	20 bit	$2^{N+1} / f_{ck}$	+
Incremental A/D Converters[98-100]	> 16 bit	$2^{N} / f_{ck}$	++
Sigma-Delta A/D Converters[101-118]	> 18 bit	$< 2^{N} / f_{ck}$	++

Figure 17.11 shows a schematic of a successive approximation A/D converter based on the charge redistribution principle. It consists of a binary weighted capacitive array, a comparator, and a successive approximation register (SAR).

At the beginning of each conversion cycle, switch S_1 is closed and the whole capacitive array is charged at the input voltage V_{in} (precharge and

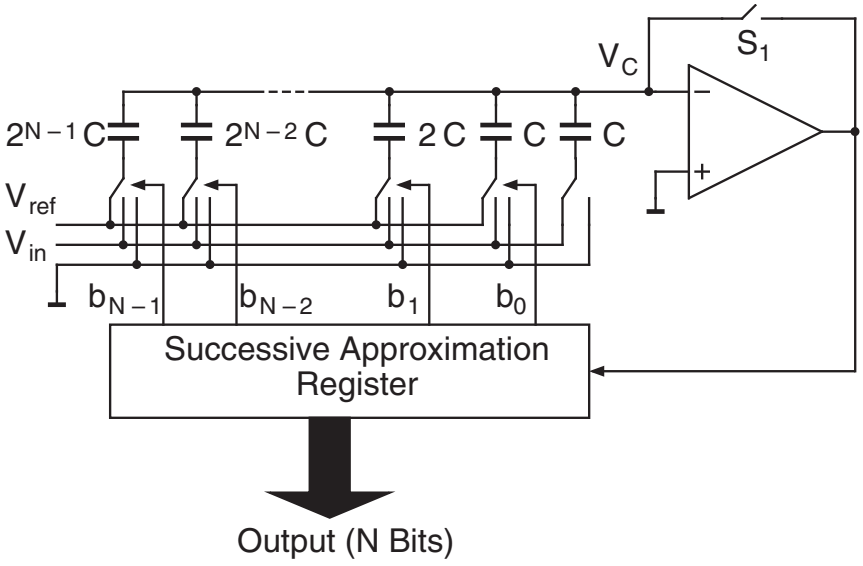

Figure 17.11 Schematic of a charge redistribution A/D converter based on the successive approximation algorithm.

auto-zero phase). Then S_1 is opened and capacitor $2^{N-1}C$, corresponding to the most significant bit (MSB), is connected to V_{ref} (b_{N-1} is set to one), while the rest of the array is connected to ground. Due to charge redistribution in the array, the voltage at the input of the comparator becomes

$$V_C = -V_{in} + \frac{V_{ref}}{2}. \tag{9}$$

If $V_C < 0$, the MSB (b_{N-1}) is confirmed to one and stored; otherwise, the MSB is set to zero. The same procedure is then repeated for the next bits. The capacitors that correspond to the already considered bits are connected to V_{ref} if the corresponding bit is one, or to ground if the corresponding bit is zero. At the end of the algorithm, V_C is therefore given by

$$V_C = -V_{in} + \sum_{i=0}^{N-1} b_i \frac{V_{ref}}{2^{N-i}}, \tag{10}$$

with $b_{N-1} \cdots b_0$ denoting the digital representation of the input signal.

Successive approximation A/D converters are widely used in sensor applications, especially for portable or battery-operated devices, in view of their low power consumption. However, because they rely on accurate analog component matching, their performance may degrade when the chip is exposed to aggressive post-processing steps or environmental conditions. By contrast, flash, half-flash, subranging, and pipeline A/D converters, although very useful for image sensing applications, are definitely impractical for low-frequency sensor applications, mainly because of their complexity.

Oversampling allows the resolution of an A/D converter to be improved by increasing the sampling frequency. This method alone is not very efficient, however, because we must quadruple the oversampling ratio M to gain one bit of resolution (or to attenuate the in-band quantization noise by 6 dB, according to Eq. (8). Better efficiency can be obtained by pushing part of the quantization noise outside the baseband while maintaining the oversampling ratio (M) constant, as shown in Fig. 17.12.

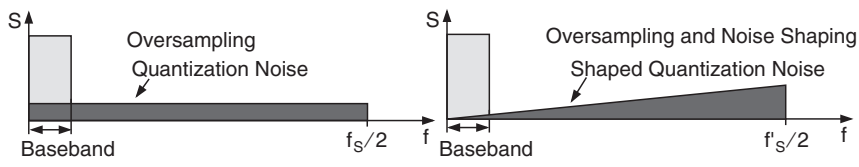

Figure 17.12 Noise shaping effect.

This effect, called noise shaping, can be achieved by introducing a suitable negative feedback around the quantizer, which modifies the transfer functions for the input signal (H_S) and for the quantization noise (H_Q).

In particular, when $H_S = 1$ and $H_Q = (1 - z^{-1})^L$, the oversampled A/D converter is called an Lth order sigma-delta ($\Sigma\Delta$) modulator. Thanks to the noise shaping effect, high-resolution $\Sigma\Delta$ modulators with a reasonable oversampling ratio can be realized using a single-bit quantizer (actually, a latched comparator). The quantization noise power spectral density in this case is given by[116-118]

$$S_Q = \frac{\Delta^2}{6f_S}\left[2\sin\left(\frac{\pi f}{f_S}\right)\right]^{2L}. \tag{11}$$

As usual, by integrating S_Q over the baseband, we can calculate the total in-band quantization noise power as

$$P_Q = \int_0^B S_Q df \cong \frac{\Delta^2\pi^{2L}}{12(2L+1)M^{2L+1}}. \tag{12}$$

The maximum signal-to-noise ratio (the signal-to-noise ratio calculated using the maximum signal amplitude $\Delta/2$) is therefore given by

$$SNR_{\max} = \frac{\Delta^2/8}{P_Q} = \frac{3(2L+1)M^{2L+1}}{2\pi^{2L}}. \tag{13}$$

The *SNR* is often used as figure of merit to quantify the accuracy of an A/D converter as an alternative to the number of significant bits (or resolution), *N*. From the *SNR*, we can easily calculate *N* as

$$N = \ln_2\left(\sqrt{\frac{2}{3}SNR}+1\right) \cong \frac{1}{2}\ln_2\left(\frac{2}{3}SNR\right) = \frac{SNR|_{\mathrm{dB}}}{6} - 0.292. \tag{14}$$

To remove the out-of-band shaped quantization noise efficiently, the low-pass decimating filter that follows an Lth order $\Sigma\Delta$ modulator must be at least of order $L + 1$. Usually, it consists of a "sinc" filter with a transfer function

$$H_D = \left[\frac{1-z^{-D}}{D\left(1-z^{-1}\right)}\right]^{L+1}. \tag{15}$$

The most interesting oversampled A/D converters for sensor applications are first- and second-order ΣΔ modulators. Due to severe stability problems, which degrade the performance, reliability, and robustness of third-order or higher order modulators, their use in microsensor interfaces is generally impractical.

Figure 17.13 shows the block diagram and the linearized model of a first-order ΣΔ modulator. Due to the minimum number of analog components required (an integrator and a latched comparator), first-order ΣΔ modulators are the best candidates for sensor applications. However, because limit cycles (caused by the correlation between input signal and quantization noise) produce unpredictable noise tones in the baseband and degrade the SNR of the circuit, first-order modulators are not often used. Noise tones can be attenuated by introducing a high-frequency dither signal, which makes the input waveform sufficiently chaotic. However, this solution reduces the dynamic range of the modulator and complicates its design.

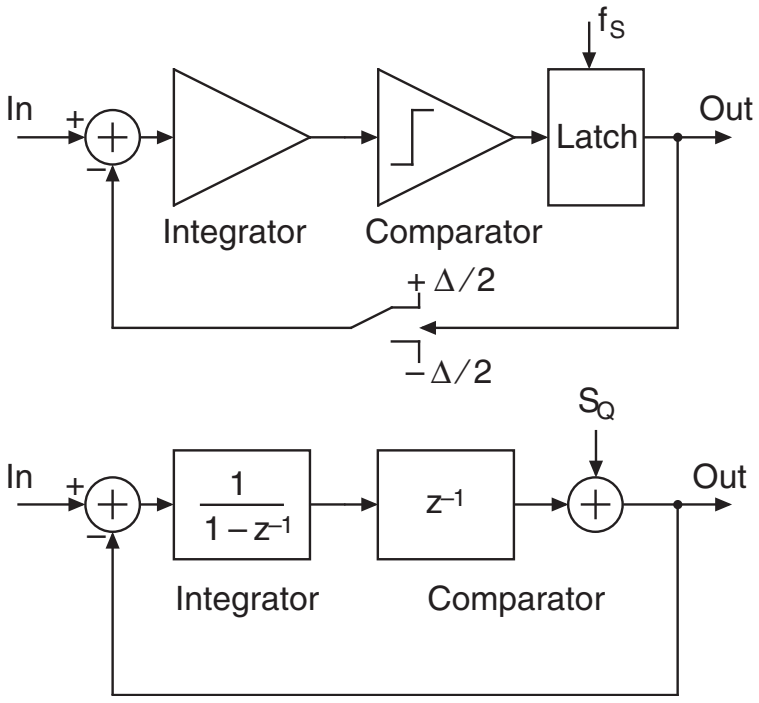

Figure 17.13 Block diagram and linearized model of a first-order sigma-delta modulator.

Another approach to solving the problem of limit cycles consists of resetting the integrator of the first-order ΣΔ modulator before each conversion cycle. The block diagram of such a circuit, called an incremental A/D converter, is shown in Fig. 17.14. Because of the periodic reset, the behavior of this circuit is deterministic rather than stochastic (i.e., for equal input signals, we obtain equal output bitstreams). Moreover, the decimating filter can be reduced to a simple up/down counter.

The incremental conversion algorithm is described by

$$\begin{cases} U_0 = In \\ U_{k+1} = U_k + \left[In - (-1)^{Q_k+1} \dfrac{\Delta}{2} \right], \end{cases} \tag{16}$$

where U and Q denote the output signals of the integrator and the comparator, respectively, and k denotes the current clock period. The N bit digital output signal obtained after 2^N clock periods is therefore given by

$$Out = 2^{N+1} \frac{In}{\Delta}. \tag{17}$$

Second-order ΣΔ modulators are much less sensitive to limit cycles than their first-order counterparts because the quantization noise is a more complex function of the design parameters. Consequently, they are less correlated to the input signal. Also, given the higher order noise shaping, they allow the same resolution to be achieved with a lower oversampling ratio, as shown in Fig. 17.15. The block diagram and the linearized model of a second-order ΣΔ modulator are shown in Fig. 17.16. The circuit con-

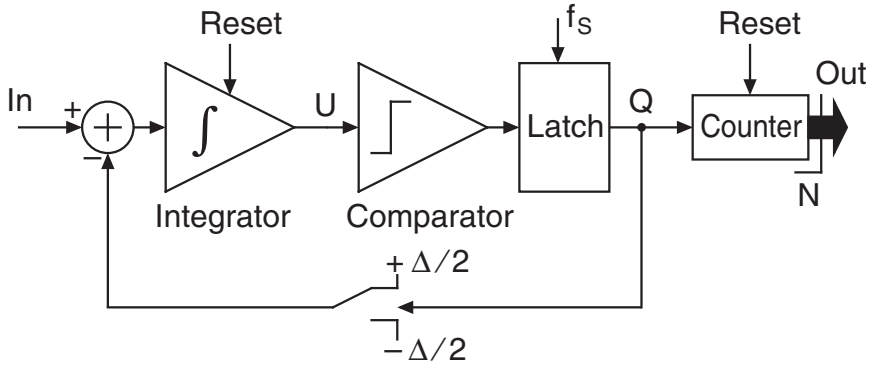

Figure 17.14 Block diagram of an incremental A/D converter.

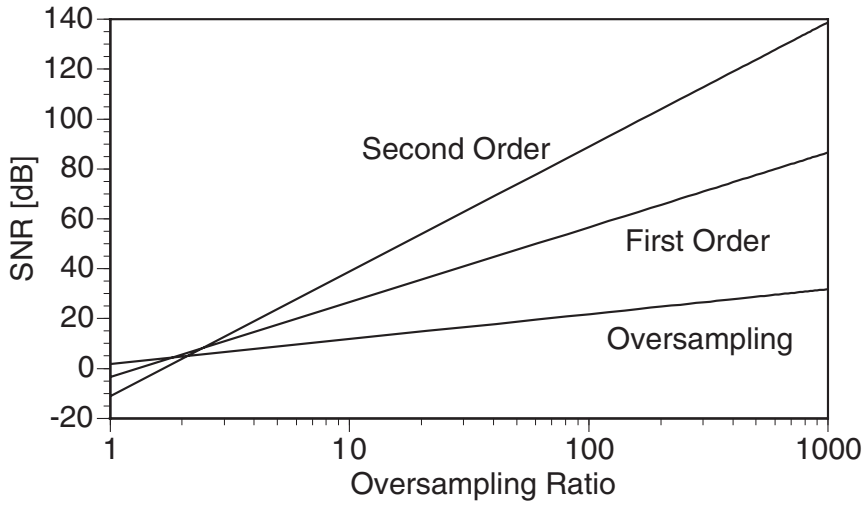

Figure 17.15 SNR versus oversampling ratio curves for different kinds of oversampled A/D converters.

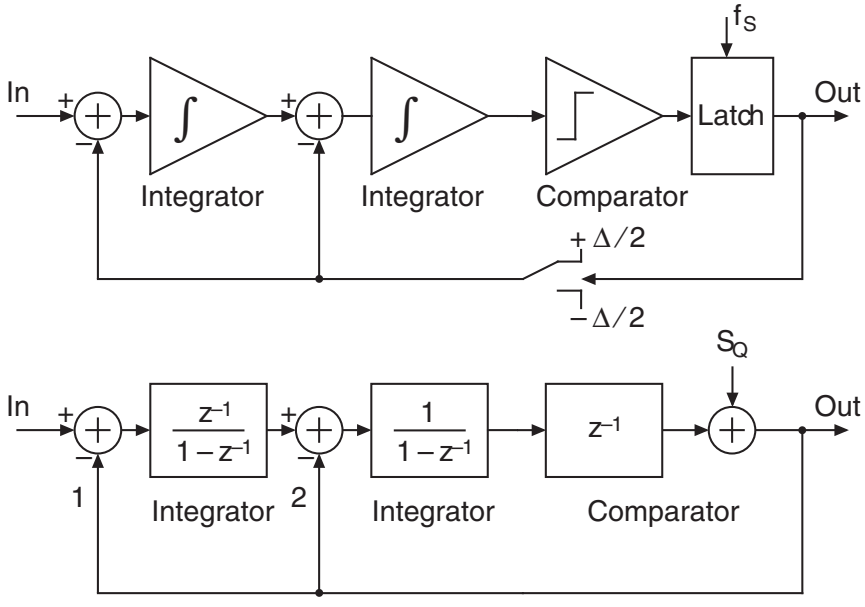

Figure 17.16 Block diagram and linearized model of a second-order sigma-delta modulator.

sists of two integrators and a comparator arranged in a closed-loop topology. Moreover, to ensure stability, a second feedback path connects the output of the comparator to the input of the second integrator.

Second-order ΣΔ modulators have been intensively used to realize microsensor interfaces because they can maintain a high level of robustness against aging and degradation by trading analog component accuracy with speed of operation. Moreover, they can be easily reconfigured to accept signals from different kinds of sensors.

As an example, consider the fourth-order, single-loop, single-bit sigma-delta modulator reported by Brigati *et al.*[115] The block diagram and the chip photograph of this circuit are shown in Figs. 17.17 and 17.18, respectively; the performance achieved is summarized in Table 17.12.

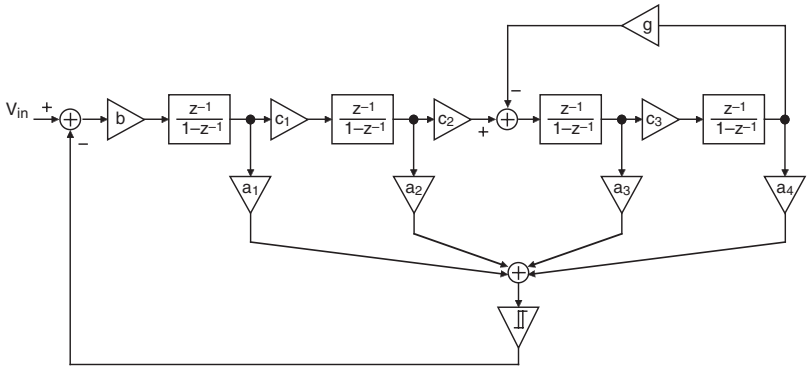

Coefficients b, c_1	0.4
Coefficient c_2	0.3
Coefficient c_3	0.1
Coefficients a_1, a_2	2
Coefficients a_3, a_4	1.5
Coefficient	0.0025

Figure 17.17 Fourth-order, single-loop, single-bit sigma-delta modulator reported by Brigati *et al.*[115]

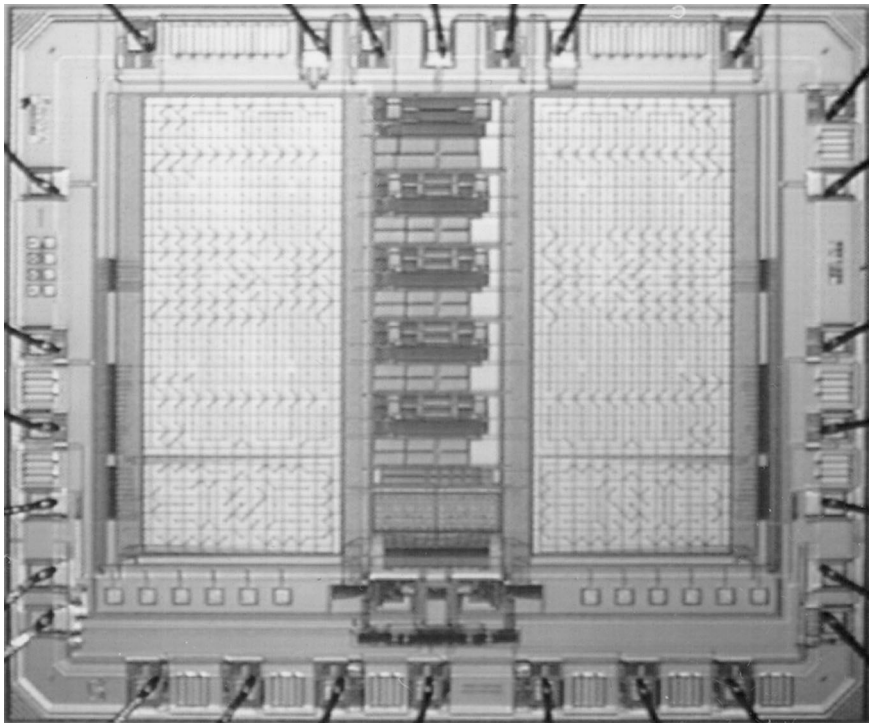

Figure 17.18 Chip micrograph of the fourth-order sigma-delta modulator reported by Brigati *et al.*[118]

Table 17.12 Features of the Fourth-Order Sigma-Delta Modulator Reported by Brigati *et al.*[118]

Parameter	Value
Application	Sensor networks
Power consumption	50 mW
Input voltage range (peak-to-peak, differential)	2 V
Bandwidth	400 Hz
Sampling frequency	256 kHz
Noise power in band	–116.9 dB
Signal-to-noise ratio at full-scale signal	104.9 dB
Resolution	17.1 bits
Chip size (including pads)	3.2 x 3.8 mm

17.7 DIGITAL PROCESSING AND OUTPUT INTERFACE

In modern microsensor systems, most of the signal processing is performed in the digital domain. This section presents the most important functions typically included in microsensor systems, with particular emphasis on the wired and wireless output interfaces.

17.7.1 Digital Signal Processing

The most important signal processing functions required for sensor applications are filtering, calibration, and control. Filtering is obviously used to limit signal bandwidth and remove out-of-band spurs or to decimate the output signal of oversampled A/D converters. No particular solution needs to be adopted to implement filters for microsensor applications: Standard digital signal processing and design techniques can be used. Thus this topic will not be considered in detail in this chapter.

The response of integrated sensors is often nonlinear. In many cases, therefore, interface circuits have to include a calibration section to linearize the transfer characteristic of the sensor, avoiding the undesirable and unpredictable effects due to nonlinear terms. Moreover, since aging often modifies the response of the sensor during the lifetime of the device, the programmability of the calibration function is also important.

Linearization and calibration are typically implemented in the digital domain to exploit the flexibility of digital signal processing. The most common techniques for sensor calibration are based on lookup tables or polynomial correction.[119-120]

The last but not least important function typically implemented digitally in microsensor systems is the control of the system operation. This includes the timing generation, the selection of the mode of operation (for example, acquisition, calibration, transmission, and self-test), and the generation of the feedback signal for adjusting the sensor or analog front-end characteristics, mentioned in Section 17.4.

17.7.2 Wired Output Interfaces

A difficult and important task in large measurement and control systems is communication between a central computer and the sensors or the

sensor subsystems, which are widely distributed throughout a plant, a building, or a car. The sensor output signals typically have different formats and may not be compatible with the input format of the central computer. Moreover, the number of wires involved can be very large, thus introducing cost and reliability problems.

Serial bus systems are the best candidates to solve these problems, since they require a minimum number of wires and allow simple transmission protocols to be implemented. Several serial bus standards have been proposed in recent years. Among them, the Philips I^2C (Inter-IC) bus system has been specially developed to interconnect integrated circuits, including sensors.[121,122] This system allows relatively small distance data transmission through a serial connection using only four lines, namely two power supply lines, a clock line, and a serial data/address line (Fig. 17.19). The maximum transfer rate is 100 kbits/sec. Each device connected to the bus has its own unique 7-bit address and can operate as a transmitter or a receiver. A master starts the data transfer on the bus and generates the required clock signal. At the same time, any bus member, addressed by the master, is considered a slave. The I^2C bus is a multimaster bus, since more than one device can initiate and terminate a data transmission. However, to avoid degradation of the message, only one device at a time can be the master.

A simplified version of the I^2C bus system, called I^2S[122], has been recently developed especially for sensor applications. In this case, the transmission is controlled by a single master (typically a microprocessor), which interrogates the various slaves (typically the sensors).

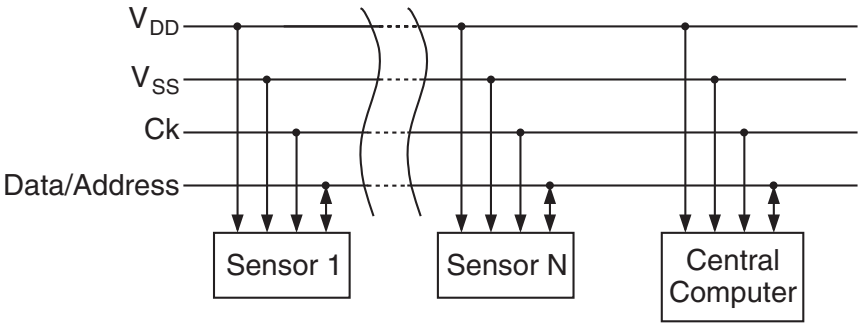

Figure 17.19 Block diagram of the I^2C bus system.

Finally, depending on the application, specific bus interfaces can be used and possibly be compatible with standard computer systems. Among them, we can cite the SPI bus, the PCI bus, the VXI bus, and the Ethernet.[123-125]

17.7.3 Wireless Output Interfaces

In the past few years, new technologies based on infrared or radio transceivers have emerged to interconnect devices without using wires. These technologies are obviously very interesting for microsystem applications, since they allow great reductions in wiring costs.

The most promising approach for wireless interfaces, especially when short-range interconnections (less than 10 m) are required, is the Bluetooth standard.[126] Table 17.13 summarizes the most important features of the Bluetooth interface. Several fully integrated Bluetooth transceivers are available on the market, either as commercial parts or as IP blocks[127-130] to be included in custom integrated circuits, thereby allowing the wireless connection feature to be included in microsystems or micromodules without considerable design effort.

Other solutions for wireless interconnections, especially for applications operating over longer ranges, are based on cellular phone standards (GSM, UMTS, DECT)[131] or on wireless LANs (IEEE 802.11b or others).

Table 17.13 Features of the Bluetooth Standard

Parameter	**Value**
Frequency band	2.4 GHz
Operating range	10 m
Channel bandwidth	1 MHz
Number of channels	79
Modulation	GFSK
Point-to-point and point-to-multipoint connections	Yes
Fully integrated transceivers in standard technologies	Yes

17.8 CONCLUSIONS

This chapter has addressed the most important issues in the design of sensor interface circuitry and microsystems. The considerations presented show how essential interface circuits are in compensating for sensor shortages and increasing the functionality of microsensor systems. However, designing good interface circuits is not enough to realize microsensor systems with optimal performance and minimum risk. In fact, it is also very important to consider interface circuitry, packaging, and testing issues, right from the design of the very first sensor. All of these aspects have to be taken into account at the specification level, with the objective of creating an optimal system that is not necessarily simply the interconnection of optimum blocks. Although the issues related to sensors and circuitry have been considered in detail in this chapter, packaging and testing contribute significantly to the industrial success or failure of a specific microsensor system and are not less important.

We hope that the world of microsensor system designers will continue to grow in the future under the impetus provided by sales of an ever-increasing number of microsensors and micromodules.

References

1. H. Baltes, "CMOS as sensor technology," *Sensors and Actuators A,* 37–38:51–56 (1993)
2. S. Middelhock and S. A. Audet, *Silicon Sensors*, Academic Press, London (1989)
3. H. Baltes, D. Moser, E. Lenggenhager, O. Brand, and D. Jaeggi, "Thermomechanical microtransducers by CMOS and micromachining," *Micromechanical Sensors, Actuators and Systems*, vol. DSC-32, ASME, New York, NY (1991), pp. 61–75
4. H. Baltes, O. Paul, J. G. Korvink, M. Schmeider, J. Bühler, N. Schneeberger, D. Jaeggi, P. Malcovati, M. Hornung, A. Häberli, M. von Arx, F. Mayer, and J. Funk, "IC MEMS microtransducers," *IEDM '96 Technical Digest* (1006), pp. 521–524
5. H. Baltes and O. Brand, "CMOS-based microsensors and packaging," *Sensors and Actuators A,* 92(1–3):1–9 (2001)
6. C. Hagleitner, A. Hierlemann, D. Lange, A. Kummer, N. Kerness, O. Brand, and H. Baltes, "Smart single-chip gas sensor microsystem," *Nature*, 414(11):293–296 (2001)
7. P. Kleinschmidt and F. Schmidt, "How many sensors does a car need?," *Sensors and Actuators A*, 21:35–45 (1992)
8. B. Bertuol, "Sensors as key components for automotive systems," *Sensors and Actuators A*, 25–27:95–102 (1991)

9. I. Igarashi, "Special features of automotive on-board sensors," *Transducers '95—Eurosensors IX Digest of Technical Papers*, vol. 1, Stockholm, Sweden (1995), pp. 898–899
10. ADXL50, *Special Linear Reference Manual, Analog Devices*, Norwood, MA (1992)
11. M. Aikele, K. Bauer, W. Ficker, F. Neubauer, U. Prechtel, J. Schalk, and H. Seidel, "Resonant accelerometer with self-test," *Sensors and Actuators A,* 92(1–3):161–167 (2001)
12. W. Geiger, J. Merz, T. Fischer, B. Folkmer, H. Sandmaier, and W. Lang, "The silicon angular rate sensor system DAVED(r)," *Sensors and Actuators A,* 84(3):280–284 (2000)
13. J. Binder, "New generation of automotive sensors to fulfill the requirements of fuel economy and emission control," *Sensors and Actuators A*, 31:60–67 (1992)
14. L. Civardi, U. Gatti, F. Maloberti, and G. Torelli, "An integrated CMOS interface for lambda sensor," *IEEE Trans. Vehicular Technol.*, 43:40–46 (1994)
15. M. Komachiya, S. Suzuki, T. Fujita, M. Tsuruki, S. Ohuchi, and T. Nakazawa, "Limiting-current type air-fuel ratio sensor using porous zirconia layer without inner gas chambers: proposal for a quick-startup sensor," *Sensors and Actuators B*, 73(1):40–48 (2001)
16. H. Fritsch, R. Lucklum, T. Iwert, P. Hauptmann, D. Scholz, E. Peiner, and A. Schlachetzki, "A low-frequency micromechanical resonant vibration sensor for wear monitoring," *Sensors and Actuators A*, 62(1–3):616–620 (1997)
17. C. P. O. Treutler, "Magnetic sensors for automotive applications," *Sensors and Actuators A*, 91(1–2):2–6 (2001)
18. J. Ji and K. D. Wise, "An implantable CMOS circuit interface for multiplexed microelectrode recording arrays," *IEEE J. Solid-State Circuits*, 27:433–443 (1992)
19. S. Konishi, T. Kobayashi, H. Maeda, S. Asajima, and M. Makikawa, "Cuff actuator for adaptive holding condition around nerves," *Sensors and Actuators B*, 83(1–3):60–66 (2002)
20. H. Suzuki, T. Tokuda, and K. Kobayashi, "A disposable 'intelligent mosquito' with a reversible sampling mechanism using the volume-phase transition of a gel," *Sensors and Actuators B*, 83(1–3):53–59 (2002)
21. S. Takeuchi and I. Shimoyama, "Selective drive of electrostatic actuators using remote inductive powering," *Sensors and Actuators A*, 95(2–3):269–273 (2002)
22. R. Puers, M. Catrysse, G. Vandevoorde, R. J. Collier, E. Louridas, F. Burny, M. Donkerwolcke, and F. Moulart, "A telemetry system for the detection of hip prosthesis loosening by vibration analysis," *Sensors and Actuators A*, 85(1–3):42–47 (2000)
23. G. T. Kovacs, C. W. Storment, M. Halks-Miller, C. R. Belczynski, C. C. Santina, E. R. Lewis, and N. I. Maluf, "Silicon-substrate microelectrode arrays for parallel recording of neural activity in peripherals and cranial nerves," *IEEE Trans. Biomedical Eng.,* 41:567–576 (1994)

24. S. Wu, Q. Lin, Y. Yuen, and Y.-C. Tai, "MEMS flow sensors for nano-fluidic applications," *Sensors and Actuators A*, 89(1–2):152–158 (2001)
25. A. Glaninger, A. Jachimowicz, F. Kohl, R. Chabicovsky, and G. Urban, "Wide range semiconductor flow sensors," *Sensors and Actuators A*, 85(1–3):139–146 (2000)
26. E. Yoon and K. D. Wise, "An integrated mass flow sensor with on-chip CMOS interface circuit," *IEEE Trans. Electron Devices*, ED-39:1376–1386 (1992)
27. D. Harwood, "Something in the air electronic nose," *IEE Review*, 47(1):10–14 (2001)
28. P. I. Neaves and J. V. Hatfield, "A new generation of integrated electronic noses," *Sensors and Actuators B*, 27(1–3):223–231 (1995)
29. J. G. Ryan;L. Barry, C. Lyden, J. Alderman, B. Lane, L. Sciffner, J. Boldt, H. Thieme, "A CMOS chip-set for detecting 10ppb concentrations of heavy metals," *IEEE ISSCC '95 Digest of Technical Papers*, San Francisco, CA (1995), pp. 158–159
30. G. C. Temes and K. Haug, "Improved offset compensated schemes for switched-capacitor circuits," *Electronics Letters*, 20:508–509 (1984)
31. K. Haug, F. Maloberti, and G. C. Temes, "SC integrators with low finite gain sensitivity," *Electronics Letters*, 21:1156–1157 (1985)
32. R. Gregorian and G. C. Temes, *Analog MOS Integrated Circuits for Signal Processing*, Wiley, New York (1986)
33. K. C. Hsieh, P. R. Gray, D. Senderowicz, and D. G. Messerschmitt, "A low-noise chopper-stabilized differential switched-capacitor filtering technique," *IEEE J. Solid-State Circuits*, 16:708–715 (1981)
34. M. Tuthill, "A switched-current, switched-capacitor temperature sensor in 0.6 μm CMOS," *IEEE J. Solid-State Circuits*, 33(7):1117–1122 (1998)
35. M. Kayal and Z. Randjelovic, "Auto-zero differential difference amplifier," *Electronics Letters*, 36(8):695–696 (2000)
36. P. Malcovati, C. Azeredo Leme, R. Lenggenhager, F. Maloberti, and H. Baltes, "Low noise multirate SC read-out circuitry for thermoelectric integrated infrared sensors," *IEEE Trans. Instr. and Meas.*, 44:795–798 (1995)
37. A. Bakker, K. Thiele, and J. H. Huijsing, "A CMOS nested-chopper instrumentation amplifier with 100-nV offset," *IEEE J. Solid-State Circuits*, 35(12):1877–1883 (2000)
38. A. Bilotti and G. Monreal, "Chopper-stabilized amplifiers with a track-and-hold signal demodulator," *IEEE Trans. Circ. and Syst. I*, 46(4):490–495 (1999)
39. A. Schaufelbühl, N. Schneeberger, U. Münch, M. Waelti, O. Paul, O. Brand, H. Baltes, C. Menolfi, Q. Huang, E. Doering, and M. Loepfe, "Uncooled low-cost thermal imager based on micromachined CMOS integrated sensor array," *IEEE J. MEMS.*, 10:503–510 (2001)
40. C. Menolfi and Q. Huang., "A fully integrated, untrimmed CMOS instrumentation amplifier with submicrovolt offset," *IEEE J. Solid-State Circuits*, 34:415–420 (1999)

41. B. J. Pichler, W. Pimpl, W. Buttler, L. Kotoulas, G. Boning, M. Rafecas, E. Lorenz, and S. I. Ziegler, "Integrated low-noise low-power fast charge-sensitive preamplifier for avalanche photodiodes in JFET-CMOS technology," *IEEE Trans. Nucl. Sci.*, 48(6):2370–2374 (2001)
42. G. C. M. Meijer and V. P. Iordanov, "SC front-end with wide dynamic range," *Electronics Letters*, 37(23):1377–1378 (2001)
43. W. J. Marble and D. T. Comer, "Analysis of the dynamic behavior of a charge-transfer amplifier," *IEEE Trans. Circ. and Syst. I*, 48(7):793–804 (2001)
44. T. Kajita, G. C. Tentes, and U. K. Moon, "Correlated double sampling integrator insensitive to parasitic capacitance," *Electronics Letters*, 37(3):151–153 (2001)
45. Y. Hu, G. Deptuch, R. Turchetta, and C. Guo, "A low-noise, low-power CMOS SOI readout front-end for silicon detector leakage current compensation with capability," *IEEE Trans. Circ. and Syst. I*, 48(8):1022–1030 (2001)
46. A. Blanco, N. Carolino, P. Fonte, and A. Gobbi, "A new front-end electronics chain for timing RPCs," *IEEE Trans. Nuclear Science*, 48(4):1249–1253 (2001)
47. C. Guazzoni, M. Sampietro, A. Fazzi, and P. Lechner, "Embedded front-end for charge amplifier configuration with sub-threshold MOSFET continuous reset," *IEEE Trans. Nucl. Sci*., 47(4):1442–1446 (2000)
48. C. Kapnistis, K. Misiakos, and N. Haralabidis, "A low noise small area self switched CMOS charge sensitive readout chain," *IEEE Trans. Nucl. Sci*., 46(3):133–138 (1999)
49. H. H. Kim, S. Chandrasekhar, C. A. Burrus, Jr., and J. Bauman, "A Si BiCMOS transimpedance amplifier for 10-Gb/s SONET receiver," *IEEE J. Solid-State Circuits*, 36(5):776 (2001)
50. K. Chin-Wei, H. Chao-Chil, Y. Shih-Cheng, and C. Yi-Jen, "2 Gbit/s transimpedance amplifier fabricated by 0.35 ∝m CMOS technologies," *Electronics Letters*, 37(19):1160 (2001)
51. H. Barthelemy, I. Koudobine, and D. Van Landeghem, "Bipolar low-power operational transresistance amplifier based on first generation current conveyor," *IEEE Trans. Circ. and Syst. II*, 48(6):625 (2001)
52. G. Palmisano and S. Pennisi, "Dynamic biasing for true low-voltage CMOS class AB current-mode circuits," *IEEE Trans. Circ. and Syst. II*, 47(12):1575 (2000)
53. C. Feng-Tso and C. Yi-Jen, "Bandwidth enhancement of transimpedance amplifier by a capacitive-peaking design," *IEEE J. Solid-State Circuits*, 34(8):1170 (1999)
54. A. Pullia, C. Fiorini, E. Gatti, A. Longoni, and W. Buttler, "ROTOR: the VLSI switched current amplifier for high-rate high-resolution spectroscopy with asynchronous event occurrence," *IEEE Trans. Nucl. Sci*., 45(6):3183 (1998)
55. C. Petri, S. Rocchi, and V. Vignoli, "High dynamic CMOS preamplifiers for QW diodes," *Electronics Letters*, vol. 34, n. 9, pp. 878 (1998)

56. G. Palmisano, G. Palumbo, and S. Pennisi, "High-drive CMOS current amplifier," *IEEE J. Solid-State Circuits*, 33(2):236 (1998)
57. C. Toumazou, J. B. Huges, and N. C. Battersby (eds.), *Switched Currents—An Analog Technique for Digital Technology*, Peter Peregrinus, London (1993)
58. A. Simoni, G. Torelli, F. Maloberti, A. Sartori, M. Gottardi, and L. Gonzo, "A 256 x 256-pixel CMOS digital camera for computer vision with 32 algorithmic ADC's on-board," *IEE Proceedings—Part G*, 146:184–190 (1999)
59. D. Bolliger, P. Malcovati, A. Häberli, P. Sarro, F. Maloberti, and H. Baltes, "Integrated ultraviolet sensor system with on-chip 1 Gtransimpedance amplifier," *IEEE ISSCC '96 Digest of Technical Papers*, San Francisco, USA (1996), pp. 328–329
60. S. Ekelof, "The genesis of the Wheatstone bridge," *Eng. Sci. and Education J.*, 10(1):40 (2001)
61. D. J. Yonce, P. P. Bey, Jr., and T. L. Fare, "A DC autonulling bridge for real-time resistance measurement," *IEEE Trans. Circ. and Syst. I*, 47(3):278 (2000)
62. D. W. Braudaway, "Precision resistors: a review of the techniques of measurement, advantages, disadvantages, and results," *IEEE Trans. Instr. and Meas.*, vol. 48, n. 5, pp. 888 (1999)
63. L. Xiujun and G. C. M. Meijer, "A smart and accurate interface for resistive sensors," *IEEE Trans. Instr. and Meas.,* 50(6):1651 (2001)
64. V. Ferrari, D. Marioli, and A. Taroni, "Oscillator-based interface for measur-and-plus-temperature readout from resistive bridge sensors," *IEEE Trans. Instr. and Meas.*, 49(3):590 (2000)
65. V. Ferrari, C. Ghidini, D. Marioli, and A. Taroni, "Oscillator-based signal conditioning with improved linearity for resistive sensors," *IEEE Trans. Instr. and Meas.*, 47(1):298 (1998)
66. S. Xiaojing, H. Matsumoto, and K. Murao, "A high-accuracy digital readout technique for humidity sensor," *IEEE Trans. Instr. and Meas.*, 50(5):1282 (2001)
67. S. Ogawa, Y. Oisugi, K. Mochizuki, and K. Watanabe, "A switched-capacitor interface for differential capacitance transducers," *IEEE Trans. Instr. and Meas.*, 50(5):1301 (2001)
68. G. C. M. Meijer and V. P. Iordanov, "SC front-end with wide dynamic range," *Electronics Letters*, 37(23):1378 (2001)
69. H. Morimura, S. Shigematsu, and K. Machida, "A novel sensor cell architecture and sensing circuit scheme for capacitive fingerprint sensors," *IEEE J. Solid-State Circuits*, 35(5):724 731 (2000)
70. W. Bo, K. Tetsuya, S. Tao, and G. Temes, "High-accuracy circuits for on-chip capacitive ratio testing and sensor readout," *IEEE Trans. Instr. and Meas.*, 47(1):20 (1998)
71. J. T. Kung and H. S. Lee, "An integrated air-gap-capacitor pressure sensor and digital readout with sub-100 attfarad resolution," *IEEE J. MEMS*, 1:121–129 (1992)

72. A. Gola, N. Bagnalasta, P. Bendiscioli, E. Chiesa, S. Delbò, E. Lasalandra, F. Pasolini, M. Tronconi, T. Ungaretti, and A.Baschirotto, "A MEMS-based rotational accelerometer for HDD applications with 2.5 rad Ú sec resolution and digital output," *Proc. ESSCIRC '01* (2001), pp. 336–339
73. J. C. Candy and O. Benjamin, "The structure of quantization noise from sigma-delta modulation," *IEEE Trans. Communication*, 29:1316–1323 (1981)
74. J. C. Candy, "Decimation for sigma-delta modulation," *IEEE Trans. Communication*, 34:249–258 (1986)
75. C. K. K. Yang, V. Stojanovic, S. Modjtahedi, M. A. Horowitz, and W. F. Ellersick, "A serial-link transceiver based on 8-GSamples/s A/D and D/A converters in 0.25-µm CMOS," *IEEE J. Solid-State Circuits*, 36(11):1684–1692 (2001)
76. V. Vujicic, "Generalized low-frequency stochastic true RMS instrument," *IEEE Trans. Instr. and Meas.*, 50(5):1089–1092 (2001)
77. M. Choi and A. A. Abidi, "A 6-b 1.3-Gsample/s A/D converter in 0.35-µm CMOS," *IEEE J. Solid-State Circuits*, 36(12):1847–1858 (2001)
78. K. Nagaraj, D. A. Martin, M. Wolfe, R. Chattopadhyay, S. Pavan, J. Cancio, and T. R. Viswanathan, "A dual-mode 700-Msamples/s 6-bit 200-Msamples/s 7-bit A/D converter in a 0.25-µm digital CMOS process," *IEEE J. Solid-State Circuits*, 35(12):1760–1768 (2000)
79. D. U. Thompson and B. A. Wooley, "A 15-b pipelined CMOS floating-point A/D converter," *IEEE J. Solid-State Circuits*, 36(2):299–303 (2001)
80. L. Sumanen, M. Waltari, and K. A. I. Halonen, "A 10-bit 200-MS/s CMOS parallel pipeline A/D converter," *IEEE J. Solid-State Circuits*, 36(7):1048–1055 (2001)
81. C. Hsin-Shu, S. Bang-Sup, and K. Bacrania, "A 14-b 20-Msamples/s CMOS pipelined ADC," *IEEE J. Solid-State Circuits*, 36(6):997–1001 (2001)
82. P. Hui, M. Segami, M. Choi, C. Ling, and A. A. Abidi, "A 3.3-V 12-b 50-MS/s A/D converter in 0.6-µm CMOS with over 80-dB SFDR," *IEEE J. Solid-State Circuits*, vol. 35, n. 12, pp. 1769–1780 (2000)
83. I. E. Opris, L. D. Lewicki, and B. C. Wong, "A single-ended 12-bit 20 Msample/s self-calibrating pipeline A/D converter," *IEEE J. Solid-State Circuits*, vol. 33, n. 12, pp. 1898–1903 (1998)
84. P. Hui, M. Segami, M. Choi, C. Ling, and A. A. Abidi, "A 3.3-V 12-b 50-MS/s A/D converter in 0.6-µm CMOS with over 80-dB SFDR," *IEEE J. Solid-State Circuits,* 35(12):1769–1780 (2000)
85. K. Nagaraj, F. Chen, and T. R. Viswanathan, "Efficient 6-bit A/D converter using a 1-bit folding front end," *IEEE J. Solid-State Circuits*, 34(8):1056–1062 (1999)
86. W. Claes, W. Sansen, and R. Puers, "A 40-µA/channel compensated 18-channel strain gauge measurement system for stress monitoring in dental implants," *IEEE J. Solid-State Circuits*, 37(3):293–301 (2002)
87. G. Promitzer, "12-bit low-power fully differential switched capacitor non-calibrating successive approximation ADC with 1 MS/s," *IEEE J. Solid-State Circuits*, 36(7):1138–1143 (2001)

88. S. Mortezapour and E. K. F. Lee, "A 1-V, 8-bit successive approximation ADC in standard CMOS process," *IEEE J. Solid-State Circuits*, 35(4):642–646 (2000)
89. J. M. Ingino and B. A. Wooley, "A continuously calibrated 12-b, 10-MS/s, 3.3-V A/D converter," *IEEE J. Solid-State Circuits*, 33(12):1920–1931 (1998)
90. P. Rombouts, W. De Wilde, and L. Weyten, "A 13.5-b 1.2-V micropower extended counting A/D converter," *IEEE J. Solid-State Circuits*, 36(2):176–183 (2001)
91. C. Dong-Young and L. Seung-Hoon, "Design techniques for a low-power low-cost CMOS A/D converter," *IEEE J. Solid-State Circuits*, 33(8):1244–1248 (1998)
92. C. Shu-Yuan and W. Chung-Yu, "A CMOS ratio-independent and gain-insensitive algorithmic analog-to-digital converter," *IEEE J. Solid-State Circuits*, 31(8):1201–1207 (1996)
93. R. V. Kochan, O. M. Berezky, A. F. Karachka, I. Maruschak, and O. V. Bojko, "Development of the integrating analog-to-digital converter for distributive data acquisition systems with improved noise immunity," *IEEE Trans. Instr. and Meas*., 51(1):96–101 (2002)
94. E. Raisanen-Ruotsalainen, T. Rahkonen, and J. Kostamovaara, "An integrated time-to-digital converter with 30-ps single-shot precision," *IEEE J. Solid-State Circuits*, 35(10):1507–1510 (2000)
95. A. Yufera and A. Rueda, "S^2I first-order incremental A/D converter," *Circuits, Devices and Systems, IEE Proceedings*, 145(2):78–84 (1998)
96. A. Häberli, M. Schneider, P. Malcovati, R. Castagnetti, F. Maloberti, and H. Baltes, "2D magnetic microsensor with on-chip signal processing for contactless angle measurement," *IEEE J. Solid-State Circuits*, 31(12):1902–1907 (1996)
97. J. Robert, G. C. Temes, V. Valencic, R. Dessoulavy, and P. Deval, "A 16-bit low voltage A/D converter," *IEEE J. Solid-State Circuits*, 22(2):157–163 (1987)
98. K. Tai-Haur, C. Kuan-Dar, and Y. Horng-Ru, "A wideband CMOS sigma-delta modulator with incremental data weighted averaging," *IEEE J. Solid-State Circ*uits, 37(1):11–17 (2002)
99. O. Oliaei, P. Clement, and P. Gorisse, "A 5-mW sigma-delta modulator with 84-dB dynamic range for GSM/EDGE," *IEEE J. Solid-State Circuits*, 37(1):2–10 (2002)
100. O. Bajdechi and J. H. Huijsing, "A 1.8-V delta-sigma modulator interface for an electret microphone with on-chip reference," *IEEE J. Solid-State Circuits*, 37(3):279–285 (2002)
101. C. B. Wang, "A 20-bit 25-kHz delta-sigma A/D converter utilizing a frequency-shaped chopper stabilization scheme," *IEEE J. Solid-State Circuits*, 36(3):566–569 (2001)
102. K. Vleugels, S. Rabii, and B. A. Wooley, "A 2.5-V sigma-delta modulator for broadband communications applications," *IEEE J. Solid-State Circuits*, 36(12):1887–1899 (2001)

103. K. Gulati and L. Hae-Seung, "A low-power reconfigurable analog-to-digital converter," *IEEE J. Solid-State Circuits*, 36(12):1900–1911 (2001)
104. E. Fogelman, J. Welz, and I. Galton, "An audio ADC Delta-Sigma modulator with 100-dB peak SINAD and 102-dB DR using a second-order mismatch-shaping DAC," *IEEE J. Solid-State Circuits*, 36(3):339–348 (2001)
105. K. Chien-Hung, C. Shr-Lung, H. Lee-An, and L. Shen-Iuan, "CMOS oversampling delta-sigma magnetic-to-digital converters," *IEEE J. Solid-State Circuits*, 36(10):1582–1586 (2001)
106. J. C. Morizio, I. M. Hoke, T. Kocak, C. Geddie, C. Hughes, J. Perry, S. Madhavapeddi, M. H. Hood, G. Lynch, H. Kondoh, T. Kumamoto, T. Okuda, H. Noda, M. Ishiwaki, T. Miki, and M. Nakaya, "14-bit 2.2-MS/s sigma-delta ADC's," *IEEE J. Solid-State Circ*uits, 35(7):968–976 (2000)
107. P. C. Maulik, M. S. Chadha, W. L. Lee, and P. J. Crawley, "A 16-bit 250-kHz delta-sigma modulator and decimation filter," *IEEE J. Solid-State Circuits*, 35(4):458–467 (2000)
108. G. J. Gomez, "A 102-dB spurious-free DR sigma-delta ADC using a dynamic dither scheme," *IEEE Trans. Circ. and Syst. II*, 47(6):531–535 (2000)
109. Y. Geerts, M. S. J. Steyaert, and W. Sansen, "A high-performance multibit delta-sigma CMOS ADC," *IEEE J. Solid-State Circuits*, 35(12):1829–1840 (2000)
110. I. Fujimori, A. Nogi, and T. Sugimoto, "A multibit delta-sigma audio DAC with 120-dB dynamic range," *IEEE J. Solid-State Circuits*, 35(8):1066–1073 (2000)
111. I. Fujimori, L. Longo, A. Hairapetian, K. Seiyama, S. Kosic, C. Jun, and C. Shu-Lap, "A 90-dB SNR 2.5-MHz output-rate ADC using cascaded multibit delta-sigma modulation at 8x oversampling ratio," *IEEE J. Solid-State Circuits*, 35(12):1820–1828 (2000)
112. E. Fogelman, I. Galton, W. Huff, and H. Jensen, "A 3.3-V single-poly CMOS audio ADC delta-sigma modulator with 538-dB peak SINAD and 105-dB peak SFDR," *IEEE J. Solid-State Circuits*, 35(3):297–307 (2000)
113. F. Medeiro, B. Perez-Verdu, and A. Rodriguez-Vazquez, "A 13-bit, 2.2-MS/s, 55-mW multibit cascade sigma-delta modulator in CMOS 0.7-μm single-poly technology," *IEEE J. Solid-State Circuits*, 34(6):748–760 (1999)
114. S. Kawahito, C. Maier, M. Schneiher, M. Zimmermann, and H. Baltes, "A 2D CMOS microfluxgate sensor system for digital detection of weak magnetic fields," *IEEE J. Solid-State Circuits*, 34(12):1843–1851 (1999)
115. S. Brigati, F. Francesconi, P. Malcovati, and F. Maloberti, "A fourth-order single-bit switched-capacitor sigma-delta modulator for distributed sensor applications," *IEEE Trans. Instr. and Meas*., 53(2):266–270 (2004)
116. R. M. Gray, "Oversampled sigma-delta modulation," *IEEE Trans. Communication*, 35:481–489 (1987)
117. J. C. Candy and G. C. Temes, "Oversampling methods for A/D and D/A conversion," in *Oversampling Delta-Sigma Data Converters* (J. C. Candy and G. C. Temes, eds.), IEEE Press, Piscataway, NJ (1991), pp. 1–29

118. S. Norsworthy, K. Schreier, and G. Temes, *Delta-Sigma Converters: Theory, Design and Simulation*, IEEE Press, Piscataway, USA (1997)
119. S. Xiaojing, H. Matsumoto, and K. Murao, "A high-accuracy digital readout technique for humidity sensor," *IEEE Trans. Instr. and Meas*., 50(5):1277–1282 (2001)
120. P. Malcovati, C. Azeredo Leme, P. O'Leary, F. Maloberti, and H. Baltes, "Smart sensor Interface with A/D conversion and programmable calibration," *IEEE J. Solid-State Circuits*, 29(8):963–966 (1994)
121. M. J Rutka, *Integrated Sensor Bus*, Delft University Press, Delft, The Netherlands (1994)
122. F. Riedijk, *Integrated Smart Sensors with Digital Bus Interface*, Delft University Press, Delft, The Netherlands (1993)
123. K. B. Lee and R. D. Schneeman, "Distributed measurement and control based on the IEEE 1451 smart transducer interface standards," *IEEE Trans. Instr. and Meas*., 49(3):627 (2000)
124. K. B. Lee and R. D. Schneeman, "Internet-based distributed measurement and control applications," *IEEE Instrumentation and Measurement Magazine*, 2(2):27 (1999)
125. M. Bertocco, F. Ferraris, C. Offelli, and M. Parvis, "A client-server architecture for distributed measurement systems," *IEEE Trans. Instr. and Meas*., 47(5):1148 (1998)
126. The Bluetooth Special Interest Group, *Specification of the Bluetooth System, Version 1.1*, *http://www.bluetooth.com* (2001)
127. R. Schneiderman, "Bluetooth's slow dawn," *IEEE Spectrum*, 37(11):65 (2000)
128. J. C. Haartsen and S. Mattisson, "Bluetooth-a new low-power radio interface providing short-range connectivity," *Proc. IEEE*, 88(10):1661 (2000)
129. J. Grilo, I. Galton, K. Wang, and R. G. Montemayor, "A 12-mW ADC delta-sigma modulator with 80 dB of dynamic range integrated in a single-chip Bluetooth transceiver," *IEEE J. Solid-State Circuits*, 37(3):278 (2002)
130. H. Darabi, S. Khorram, C. Hung-Ming, P. Meng-An, S. Wu, S. Moloudi, J. C. Leete, J. J. Rael, M. Syed, R. Lee, B. Ibrahim, M. Rofougaran, and A. Rofougaran, "A 2.4-GHz CMOS transceiver for Bluetooth," *IEEE J. Solid-State Circuits*, 36(12):2024 (2001)
131. F. Torán, D. Ramírez, A. E. Navarro, S. Casans, J. Pelegrí, and J. M. Espí, "Design of a virtual instrument for water quality monitoring across the Internet," *Sensors and Actuators B*, 76(1–3):281–285 (2001)